Applied Catalysis B: Environmental 158–159 (2014) 400–409

Contents lists available at ScienceDirect

Applied Catalysis B: Environmental

journal homepage: www.elsevier.com/locate/apcatb

Supported Co catalysts prepared as thin films by magnetron sputtering for sodium borohydride and ammonia borane hydrolysis

M. Paladini, G.M. Arzac*, V. Godinho, M.C. Jiménez De Haro, A. Fernández

Instituto de Ciencia de Materiales de Sevilla, CSIC-Univ. Sevilla, Américo Vespucio 49, Isla de la Cartuja, Seville, Spain

ARTICLE INFO

Article history:
Received 31 January 2014
Received in revised form 14 April 2014
Accepted 25 April 2014
Available online 4 May 2014

Keywords:
Sodium borohydride
Catalytic hydrolysis
Co thin films
Magnetron sputtering
Durability

ABSTRACT

Supported Co catalysts were prepared for sodium borohydride and ammonia borane hydrolysis by magnetron sputtering for the first time under different conditions. Ni foam was selected as support. Deposition conditions (time, pressure, and power) were varied to improve catalytic activity. A decrease in deposition power from 200 to 50 W, leads to a decrease in crystallite and column size and a higher activity of catalysts. The increase in deposition pressure from 1.5×10^{-2} to 4.5×10^{-2} mbar produces same effect but in this case the enhancement in activity is higher because amorphous materials were obtained. The highest activity for SB hydrolysis was 2650 ml min^{-1} $g_{cat}{}^{-1}$ for the 50 W Co 4.5 (4 h) sample ($E_a = 60 \pm 2$ kJ mol^{-1}). For AB hydrolysis activity for the 50 W Co 3.2 (4 h) sample was similar. Durability of the thin films was tested for both reactions upon cycling (14 cycles). Diluted acid washing was effective to recover the activity for sodium borohydride reaction but not for ammonia borane hydrolysis. The strong Co–NH_3 interactions explain the non-efficiency of the acid washing.

1. Introduction

Nowadays, hydrogen is considered as a potential future energy carrier owing to its high energy content, renewability and non-polluting energy release (reaction with oxygen produces water as only by-product). However, one bottleneck for the development of a hydrogen economy is the issue of hydrogen storage. Over the last decade hydrolysis of chemical hydrogen storage materials such as sodium borohydride (SB) and ammonia borane (AB) have proven to be an efficient approach for hydrogen generation [1–4]. Both hydrides are stable in dry air and easy to handle and combine low molecular weight (37.8 and 30.7 g mol^{-1} for SB and AB, respectively) with high gravimetric hydrogen content, making them very attractive. Catalyzed sodium borohydride and ammonia borane hydrolysis are safe exothermic reactions that produce hydrogen according to (1) and (2), respectively [1–4].

$$NaBH_4 + 2H_2O \rightarrow 4H_2 + NaBO_2 \quad (1)$$

$$NH_3BH_3 + 2H_2O \rightarrow NH_4{}^+ + BO_2{}^- + 3H_2 \quad (2)$$

Both spontaneous reactions are slow and need catalysts to occur at appreciable rates. One of the main obstacles for the practical application of the catalytic hydrolysis of these (SB and AB) chemical hydrogen storage materials is the need to develop efficient, economical and durable catalysts to accelerate reactions (1) and (2) [1–4]. Co based catalysts have demonstrated in the past decade to be the most advantageous and cost effective for reaction (1) [1–3,5–7] and also for reaction (2) [4–7].

From a technological and operational point of view, i.e. system and reactor design, it is highly desirable to have Co catalysts in a supported form [2,3]. Supported catalysts do not aggregate as powder catalysts and can be recovered from the reaction medium, to be reused in multi-use applications. Traditionally, Co supported catalysts have been mainly prepared by the impregnation-chemical reduction method [1–14]. In most cases, sodium borohydride is employed as reducing agent leading to the formation of Co–B materials [15–18].

Electrodeposition has also been presented as a convenient method for scale-up the production of supported Co catalysts [19,20]. However for non-conducting substrates an intermediate step for the deposition of a conductive layer is need.

Pulsed laser deposition is a PVD (physical vapor deposition) technique that has been employed for the preparation of catalysts for SB and AB hydrolysis. Co–B thin films and more recently, Co nanoparticles on a B film have been prepared by this method [21–24]. This technique allows to deposit high density granular films of different roughness with the target stoichiometry [21–25].

* Corresponding author. Tel.: +34 954489552; fax: +34 954460665.
E-mail address: gisela@icmse.csic.es (G.M. Arzac).

http://dx.doi.org/10.1016/j.apcatb.2014.04.047
0926-3373/

Magnetron sputtering is a PVD technique that allows the deposition of thin films with precise controlled thickness over a wide variety of substrates due to the low deposition temperature of the process. It can be easily scaled to industrial processes and is a low cost process without the need of precursors avoiding emissions of toxic by-products. The control of the deposition conditions allows controlling the microstructure of the coatings and sputtering conditions can be readily reproduced from run-to-run. This technique has proven before to be a versatile tool to prepare nanostructured and porous materials in our group [26–28]. To our knowledge, magnetron sputtering has not been reported as preparation technique for supported Co catalysts for sodium borohydride or ammonia borane hydrolysis before [29].

In this paper, Ni foam supported nanostructured Co coatings (Co/Ni foam) were prepared as thin films by magnetron sputtering in a wide range of conditions as catalysts for reactions (1) and (2). As a proof of concept, PTFE membranes were also used as thin film support.

Catalytic activity of the Co/Ni foam materials was tested for reactions (1) and (2) in 4.5 wt% NaOH and pure water, respectively. Activity is correlated to deposition conditions, crystallinity and nanostructure. Durability was also tested for both reactions upon cycling (14 cycles) and compared. A reactivation step consisting in dilute acid washing was also employed and the results discussed.

2. Experimental

2.1. Catalysts preparation

To investigate the influence of the different deposition parameters on the activity of the supported catalyst, Co nanostructured coatings were deposited under different pressure and dc power. Table 1 summarizes the deposition conditions employed.

The coatings were deposited using a 2″ magnetron from AJA in magnetic target configuration, from a pure cobalt target (Kurt J. Lesker 99.95% pure, 1 mm thick) under pure argon atmosphere. The base pressure before deposition was 10^{-6} mbar, and working pressures from 1.5×10^{-2} to 4.5×10^{-2} mbar of Ar were employed to prepare the coatings.

The influence of the deposition power on the microstructure and consequently on activity was investigated by changing the dc power supplied from 50 to 200 W.

The coatings were deposited directly on commercial Ni foam (Goodfellow 1.6 mm thick, 95% porosity, 20 pores cm^{-1}) and PTFE (polytetrafluoroethylene) membranes (Whatman 0.2 μm pore size, polypropylene backed). Before deposition, Ni foam or PTFE membranes were cut into $0.5 \times 0.5\ cm^2$ pieces and grouped to be used in a small reactor (see Section 2.3). Each group was weighted before and after each deposition to obtain the total mass of catalyst deposited. Depositions times of 2 and 4 h allowed to obtain different catalyst mass under similar deposition conditions.

Ni foam was washed first with ethanol and then with HCl 0.1 M in an ultrasonic bath before each synthesis. No previous treatment was done on PTFE membranes. As a reference for characterization (specially electron microscopy), in each deposition Si (1 0 0) substrates were included. The Si substrates were cleaned with acetone and dried in a nitrogen flow.

Catalysts are named by their deposition/synthesis conditions and the support. As an example, 200 W Co 1.5 (2 h) catalyst is the Ni foam supported catalyst prepared by magnetron sputtering at 200 W power and 1.5×10^{-2} mbar Ar pressure during 2 h. To avoid confusion, Table 1S (included as Supporting information) correlates catalyst name and preparation conditions. In those cases in which the support is different from Ni foam, it will be clearly indicated in the text.

2.2. Catalysts characterization

Scanning electron microscopy (SEM) was performed to study the morphology of the coatings on the different substrates and the thickness of samples deposited on Si (1 0 0) in a high resolution FEG microscope, HITACHI S4800 operating at 2 kV equipped with an EDX detector (Bruker X-Flash 4010). The microstructure of the coatings was investigated by transmission electron microscopy (TEM), performed using a Philips CM 200 microscope with 2.4 Å resolution. Cross-sectional transmission electron microscope (XTEM) specimens were prepared in the conventional way by mechanical polishing followed by Ar^+ ion milling to electron transparency of coatings deposited on Si substrates. Surface topography was investigated by atomic force microscopy (AFM) Nanotec system working in tapping mode, with Si tips of 150 kHz resonant frequency and 20 N m^{-1} spring constant. 3D surface images of 5×5 μm were acquired and analyzed with the WSxM free available software from Nanotec [30].

X-ray diffraction measurements were performed using Cu $K\alpha$ radiation in a Siemens D5000 diffractometer in a Bragg-Brentano configuration in the 2θ angle range of 20–90 degrees. The surface chemical composition of the catalyst before and after test was investigated by XPS. XPS spectra were recorded with a Leybold Heraus LH electron spectrometer using Al Ka radiation with 40 eV pass energy at normal emission take off angle. The spectra were calibrated with the position C (1s) (from contamination) signal at 284.9 eV.

2.3. Hydrogen generation (HG) test

Ni foam supported Co catalysts were tested as following: a certain amount of supported catalyst (1–8 mg) was placed at the bottom of a three necked heart-shaped flask. The flask was immersed in a water bath maintained at 23 ± 0.5 °C and connected to a 100 ml gas burette. The reactions (1) and (2) started by injecting 38 mg of SBH dissolved in 1 ml of 4.5 wt% NaOH solution or 40 mg of AB dissolved in 1 ml of MilliQ® water, respectively. The amount of generated hydrogen was measured by reading the displacement of the piston in the gas burette (gas-tight by a mercury o-ring) as a function of time. For AB hydrolysis experiments the produced gas was passed through a flask with 0.1 M H_2SO_4 solution to remove ammonia, before directing to the gas burette. No stirring was used for the experiments, except for the stirring effect of the evolved hydrogen. The HGR (Hydrogen Generation Rate, ml min^{-1}) was obtained from the slope of the plot of the volume of hydrogen evolved vs time in linear regime. Experiments were done in duplicate, and showed to be reproducible. In this paper, catalytic activity (expressed in ml min^{-1} $g_{cat}{}^{-1}$) is obtained as the slope from the plot of HGR (ml min^{-1}) as a function of the mass of supported catalyst.

To test durability, the above mentioned tests for reaction (1) and (2) were repeated for 14 times. After each test, catalyst was extracted from the reaction medium and washed with distilled water and ethanol then it was dried under a N_2 flow. When indicated, the used catalyst was washed with 10^{-4} M HCl. This acid washing is intended to eliminate the adsorbed $BO_2{}^-$ ions which produce catalyst deactivation [20,31]. Catalyst loss was evaluated after each test by weighting.

3. Results and discussion

3.1. The supported catalyst

By choosing the adequate deposition conditions, magnetron sputtered highly columnar coatings, with high surface area to be used as catalysts, can be obtained. Fig. 1 shows the morphology

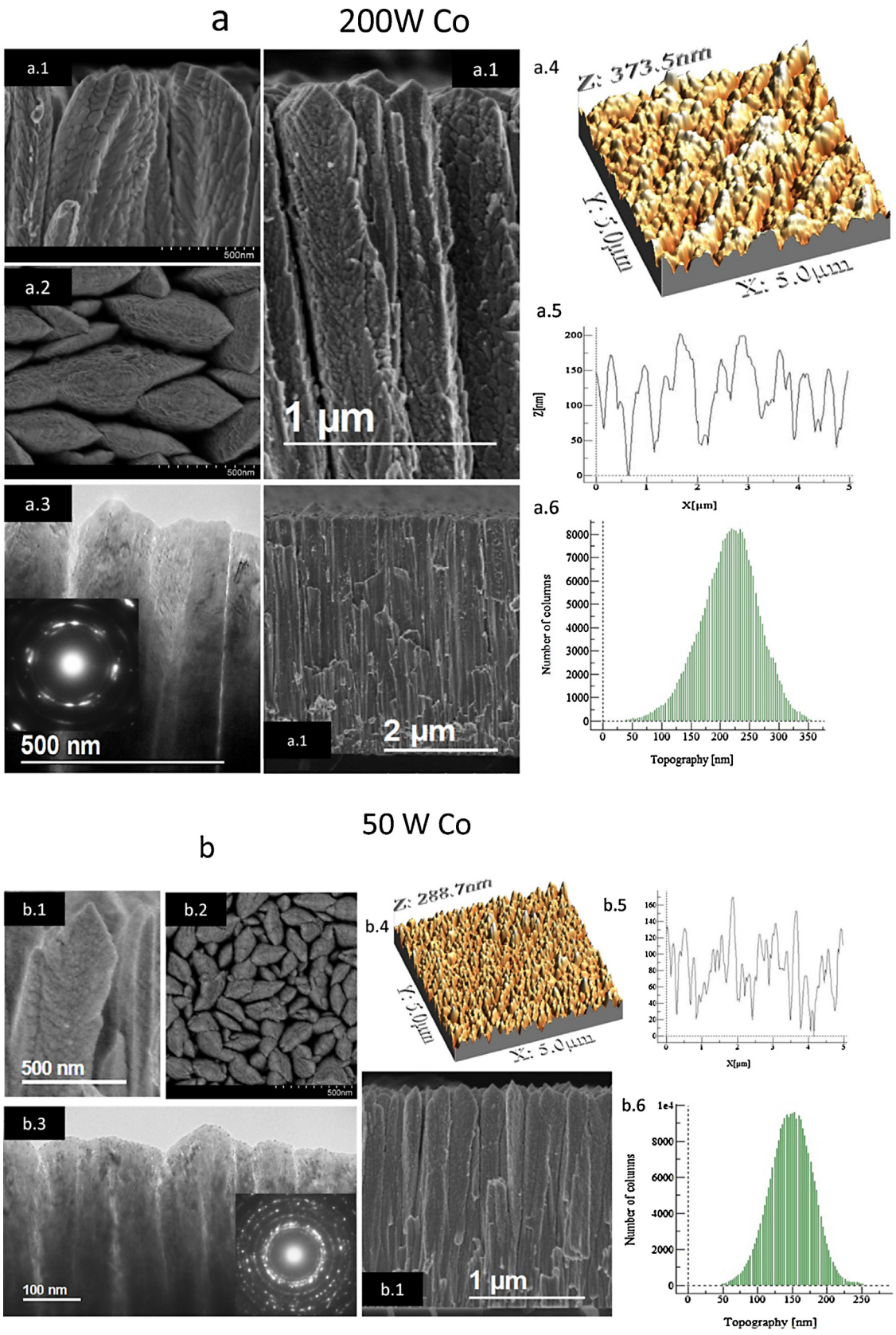

Fig. 1. (a). The 200 W Co 1.5 (2 h) thin film. (a.1) Cross sectional SEM images. (a.2) Planar SEM image. (a.3) TEM image (inset SAED). (a.4) AFM image. (a.5) Signal intensity profile of image (a.4). (a.6) Column size histogram. (b) The 50 W Co 1.5 (2 h) thin film. (b.1) Cross sectional SEM images. (b.2) Planar SEM image. (b.3) TEM image (inset SAED). (b.4) AFM image. (b.5) Signal intensity profile of image (b.4). (b.6) Column size histogram.

Table 1
Characterization of the Co thin films obtained by magnetron sputtering at 1.5×10^{-2} mbar.

Sputtering power (W)	50		200	
Deposition time (h)	2	4	2	4
Film thickness (nm)	900	2000	4100	7300
Deposition rate (nm s^{-1})	0.12	0.13	0.56	0.51
Temperature achieved during the deposition (°C)	45–55	50	120–145	150–175

and microstructure of the supported Co coatings deposited on Ni foam and silicon at 200 and 50 W, under Argon pressure of 1.5×10^{-2} mbar during 2 h.

In both cases the coatings present columnar growth, typical of magnetron sputtered coatings deposited under low adatom mobility conditions where surface shadowing governs the film growth [32]. The cross-sectional SEM and TEM micrographs (Fig. 1.a.1, 1.a.3 and 1.b.1, 1.b.3) reveal that these meso-columns are composed by nano-columns in a feather-like structure where high intra and inter-columnar porosity can be observed. TEM shows that inside the columns there is a superlattice structure perpendicular to the growth direction, corresponding to nano-columns growing tilted with respect to the growing direction. The width of the meso-columns (average values from SEM in the meso-columns highest dimension) varies from 50 to 350 nm in the case of the 50 W coatings and from 150 to 900 nm when 200 W dc power is applied. The surface topography of these samples was also investigated by AFM and is shown on Fig. 1a.4 and 1.b.4. Clear differences between the two power conditions can be observed, the sample deposited at 50 W is composed by thinner meso-columns with sharper ends than in the case of the 200 W catalyst as it can be observed by the AFM profiles. The meso-columns ends present different heights as displayed on the histograms of topography vs number of columns. For 50 W Co catalyst the majority of meso-columns have a height of 150 nm while for the 200 W it is around 225 nm.

The influence of different substrates on the coatings morphology and microstructure was investigated. Fig. 2 presents as an example a cobalt coating deposited at 200 W, on Si(1 0 0) in comparison with the same coating deposited simultaneously on nickel foam and PFTE membrane, the former a traditional support for SBH hydrolysis. Magnetron sputtering technique has proven to be able to cover efficiently these supports and conformal coatings with similar columnar structure were obtained. (On Supporting information more details on bare and covered Ni foam and PFTE membrane can be found in Fig. 1S.) The higher magnification SEM micrographs (Fig. 2 d–f)) show that the columnar microstructure of the catalyst is similar on the different substrates.

3.2. Catalytic activity of Co coatings for SB hydrolysis

Activity for SB hydrolysis was measured in 4.5 wt% NaOH solution for each prepared Ni foam supported catalyst. Results are summarized in Table 2. As an example, in Supporting information (Fig. 2S) hydrogen evolution curves and hydrogen generation rate plot as a function of the mass of catalyst are shown for the 50 W Co 3.2 (4 h) sample. For all tested catalysts, hydrogen evolution curves follow a straight line indicating zero-order kinetics in SB concentration. No induction period was detected in hydrogen evolution experiments. Thin films have shown to be stable and well adhered to the support in reaction conditions. No catalyst loss was found during hydrolysis tests.

The following sections discuss the influence of deposition power, time, and pressure on the microstructure and catalytic activity of Co coatings for SB hydrolysis.

3.2.1. Effect of deposition power

Table 2 presents the corresponding catalytic activities for deposition powers of 50 and 200 W. A significant increase on activity (from 360 to 700 ml min^{-1} $g_{cat}{}^{-1}$) is observed when deposition power decreases at 1.5×10^{-2} mbar and 2 h (entries 2a and 2d). The morphological changes between coatings deposited at different powers, presented in Fig. 1 contribute greatly to the

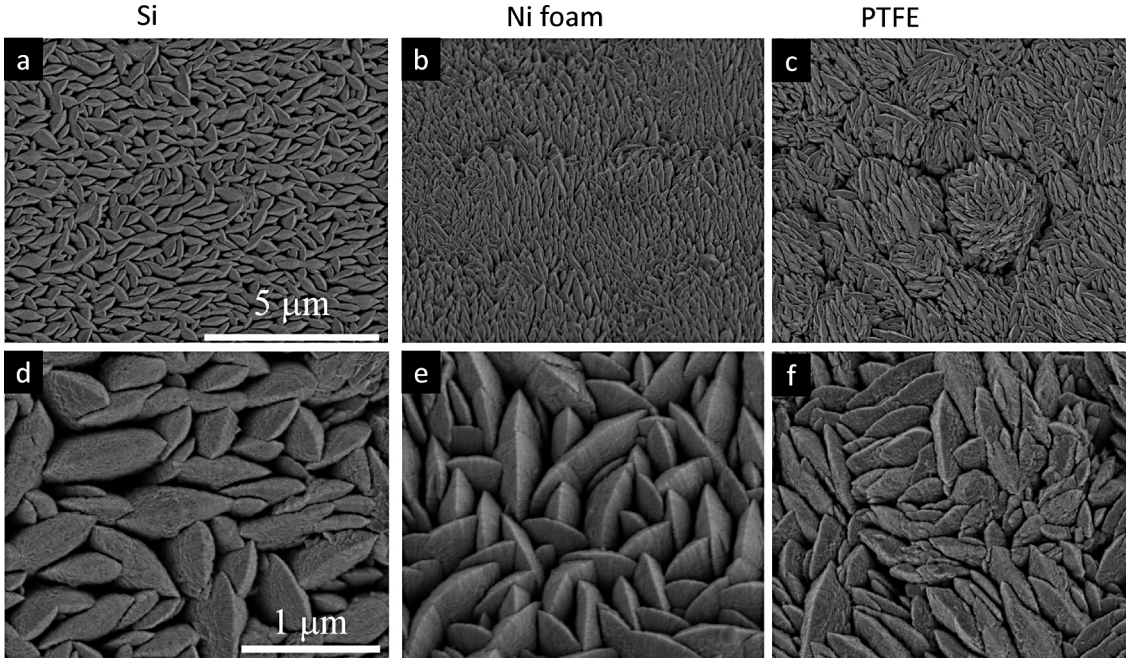

Fig. 2. Planar SEM images of 200 W Co 1.5 (2 h). (a),(d) Si supported; (b),(e) Ni foam supported; (c),(f) PTFE membrane supported. ((a–c) and (d–f) same scale bar, respectively).

Table 2
Catalytic activity (ml min^{-1} $g_{catalyst}^{-1}$) for SBH hydrolysis for the prepared Ni foam supported Co thin films as a function of deposition conditions.

Entry	Catalyst	Deposition pressure (mbar)				
		1.5×10^{-2}	2×10^{-2}	2.8×10^{-2}	3.2×10^{-2}	4.5×10^{-2}
2.a	200 W Co (2 h)	360	–	–	1350	–
2.b	200 W Co (4 h)	350	–	–	–	–
2.c	100 W Co (4 h)	500	–	–	–	–
2.d	50 W Co (2 h)	700	–	–	–	–
2.e	50 W Co (4 h)	670	570	1550	2050	2650

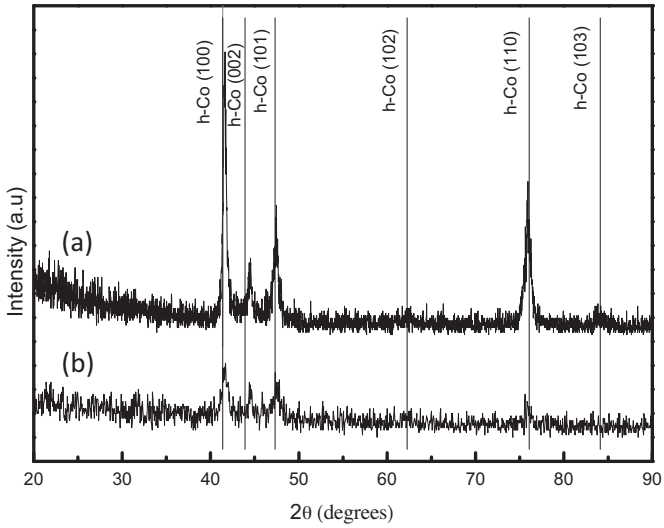

Fig. 3. XRD measurements performed on (a) 200 W Co 1.5 (2 h)/PTFE; (b) 50 W Co 1.5 (2 h)/PTFE thin films.

different activity. Column width increases with deposition power reducing the number of columns per square nanometre. The study of the effect of deposition power on supported catalysts' surface area and the number of active sites is difficult to study by BET and chemisorption measurements that require high amount of catalyst. Nevertheless, the AFM profiles on Fig. 1 show clearly a higher surface area in the case of the 50 W prepared catalyst.

On the other hand, it is known that amorphous (or nanocrystalline) Co catalysts are more catalytically active than the corresponding crystalline samples [5]. Fig. 3 shows the XRD diffractograms of the 50 W and 200 W PTFE supported cobalt catalysts. Both catalysts show peaks which can be assigned to the hcp Co phase. Scherrer analysis on both diffractograms indicates crystal sizes ((1 0 0) hcp Co) of 11 nm and 31 nm for the 50 and 200 W Co catalysts, respectively. In this range of conditions catalytic activity can be correlated to the inverse of crystal size. In fact crystal size and columns width both indicate a higher active surface area for the same amount of catalyst when decreasing deposition power. The SAED patterns (Fig. 1.a.3 and 1.b.3, inset) indicates more crystallinity in the case of the catalyst deposited at 200 W in accordance to XRD.

3.2.2. Effect of deposition time

A direct way to control the amount of supported catalyst under the same deposition conditions is by varying deposition time. However it is known that magnetron sputtered columnar films grown under low atom mobility conditions often present V-shaped columns with competitive growth, that become wider from the substrate to the surface. A considerable increase of column width with consequent decrease of inter-columnar pores would decrease total surface an influence the catalytic activity of the coatings. Table 1 shows the influence of deposition time for two different powers on film thickness and deposition rate and Fig. 4 gives an example of morphology changes from 2 to 4 h of deposition.

Deposition rate, calculated from SEM cross-sectional thickness measurements, is not affected by deposition time, increasing with the increase of power supplied (0.12–0.13 nm s^{-1} for 50 W power and 0.51–0.56 for 200 W). Fig. 4 shows a decrease of porosity and an increase of competitive columnar growth for coatings deposited at the same power and double time. The open spaces between columns observed for 2 h deposition (Fig. 4a) are occupied by competition of smaller columns for 4 h (Fig. 4b). Despite the microstructural differences between both catalysts, no significant effect was found in catalytic activity for sodium borohydride hydrolysis (Table 2, entries 2.a and 2.b). Similar results were found for 50 W Co 1.5 (2 h, 4 h) catalysts (Table 2, entries 2.d and 2.e, respectively). It seems that the significant increase of smaller mesocolumns with feather like structure is enough to increase the total surface area, compensating loss of inter-columnar active places for the catalytic reaction.

3.2.3. Effect of deposition pressure

Deposition pressure is also a well-known parameter influencing film's microstructure during magnetron sputtering growth of thin films. As a general behaviour the increase of deposition

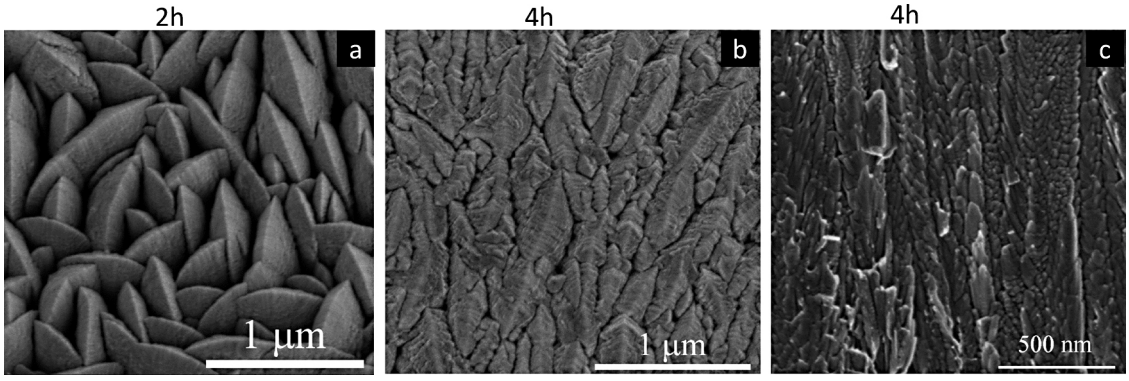

Fig. 4. Planar SEM images of (a) 200 W Co 1.5 (2 h) (b) 200 W Co 1.5 (4 h) (c) Cross sectional SEM image of (b).

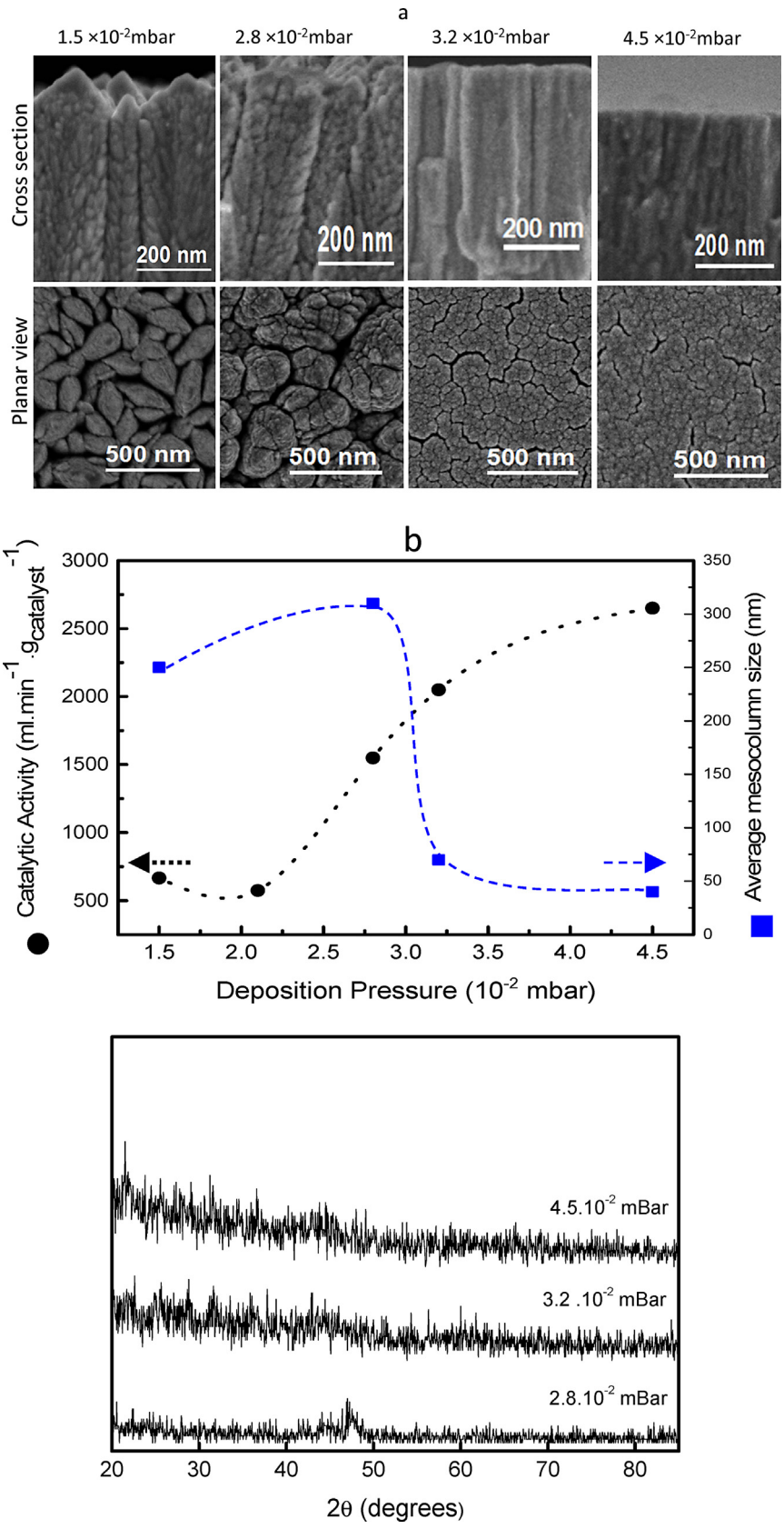

Fig. 5. (a) Cross sectional and planar SEM images of the 50 W Co (4 h) thin films as a function of deposition pressure.(b) Catalytic activity and average mesocolumn size as a function of deposition pressure and XRD difractograms for the 50 W Co (4 h) thin films.

pressure leads to the formation of granulated films that could end in a powder-like film. The effect of deposition pressure in catalytic activity and microstructure was also studied in this work. Supported Co catalysts were deposited at 50 W during 4 h on Ni foam. Deposition pressure was varied in the range of 1.5–4.5 $\times 10^{-2}$ mbar. Fig. 5a presents details of the morphological changes that occur with the increase of deposition pressure. At low pressure (1.5×10^{-2} mbar) the meso-columns (sizes ranging from 50 to 350 nm width) are composed by nano-columns with a feather like structure with big inter-columnar spaces. As the pressure increases to 2.8×10^{-2} mbar the meso-columns tend to gather in groups forming bigger units where the intercolumnar space is reduced. These units can be considered itselves as different meso-columns with sizes from 70 to 430 nm. A further increase in pressure, to 3.2×10^{-2} mbar changes the meso-columns structure from feather like to vertically aligned nano-columns. Meso-columns sizes from 20 to 120 nm can be observed by SEM. At 4.5×10^{-2} mbar the meso-columns became thinner, 10-70 nm width. This shows that column size decreases strongly with deposition power.

Catalytic activity as a function of deposition pressure for the 50 W Co (4 h) material is shown in Table 2 (entry 2.e). Fig. 5b also plots the catalytic activity as a function of deposition pressure. Up to 2×10^{-2} mbar, catalytic efficiency does not vary with pressure. Further pressure increase produces a linear increase in activity up to 3.2×10^{-2} mbar. Activity falls from the linear trend for higher deposition pressure. Fig. 5b also plots the average meso-column size as a function of deposition pressure. There is a clear correlation between deposition pressure, column size and catalytic activity. The decrease in column size (more disperse material) observed with deposition pressure directly correlates with activity.

Fig. 5b shows the XRD diffractograms of the thin films obtained as a function of pressure. The increase of deposition pressure has also an important effect on the crystallite size, since more amorphous and disperse coatings are obtained at higher pressures contributing also to the increase of catalytic activity. Similar dependency of crystallite size on deposition pressure was observed before in literature for Co-based coatings deposited by magnetron sputtering [33].

Increasing deposition pressure has demonstrated to be an efficient strategy to obtain amorphous materials (Fig. 5b) which exhibit enhanced catalytic activity in respect to those obtained by varying deposition power (Section 3.2.1, Fig. 3), with high crystallinity. This shows that the amorphous/nanocrystalline microstructure is a requirement for Co thin film catalysts to obtain higher activity.

The Arrhenius plot for 50 W Co 4.5 (4 h) catalyst, which exhibited the highest activity, is shown in Fig. 3.S (as Supporting information). The resulting activation energy (E_a) was (60 ± 2) kJ mol^{-1} which is lower than the previously reported for bulk cobalt (75 kJ mol^{-1}) [34]. For the same prepared thin film, the effect of NaOH concentration on catalytic activity was also studied. Kinetic tests were performed at 0, 4.5, 10, 20 wt% NaOH and results are shown in Fig. 4.S (as Supporting information). The plot of the normalized HGR as a function of NaOH concentration shows that activity reaches a maximum for 4.5 wt% NaOH and then decreases slowly for higher NaOH concentration. This trend, reported previously for Co and Co-B catalysts, is consistent with the mechanism proposed by Holbrook and Twist, which involves a non-catalyzed intermediate reaction which is dependent on NaOH concentration [12,35,36].

3.3. Catalytic activity for AB hydrolysis

For the 50 W Co 3.2 (4 h) sample, activity was also measured for AB hydrolysis in pure water. Fig. 6a shows the hydrogen evolution curves. Hydrogen evolution follows a straight line indicating zero-order in AB concentration with a 2–5 min induction time which decreases with the mass of catalyst. Activity was calculated from

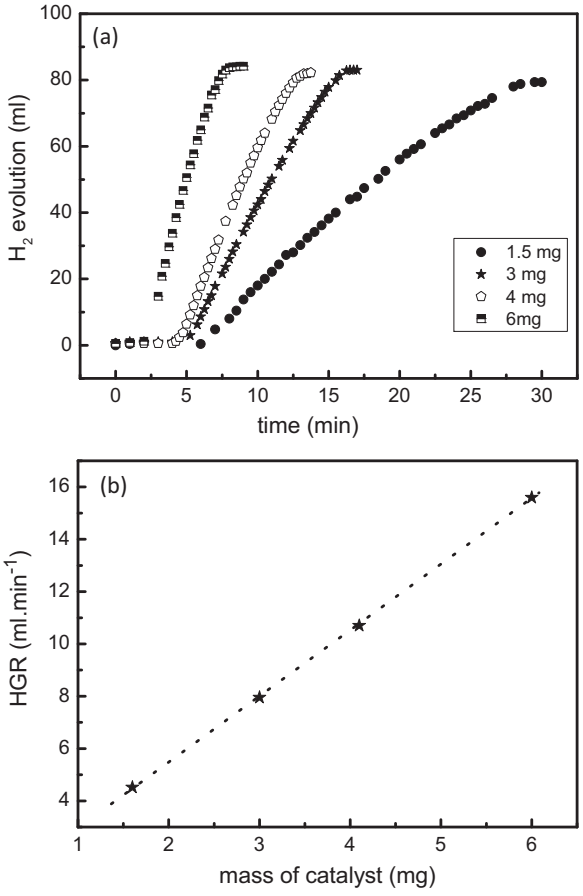

Fig. 6. (a) Hydrogen evolution curves for the 50 W Co 3.2 (4 h) catalyzed AB hydrolysis. (b) Hydrogen generation rate as a function of the mass of catalyst for the same catalyst.

de HGR vs mass plot as 2500 ml min^{-1} g_{cat}^{-1}. For the same thin film catalyst, the activity was higher for AB than for SB reaction (Table 2, entry 2.e, column 4).

The Arrhenius plot for 50 W Co 4.5 (4 h) catalyst is shown in Fig. 5.S (as Supporting information). The resulting activation energy for AB hydrolysis (E_a) was (59 ± 1) kJ mol^{-1} which is similar to the previously reported for Co/γ Al_2O_3 (62 kJ mol^{-1}) [14].

3.4. Durability upon cycling

One of the major challenges for the catalysts employed in these hydrogen-producing reactions (1) and (2), is durability upon cycling. This property is an essential requirement for the design of multi-use reactors. For this reason, durability was tested for selected Co catalysts prepared as thin films upon 14 cycles for SB and AB hydrolysis. Results are discussed below.

3.4.1. Sodium borohydride hydrolysis

Durability of the 200 W Co 1.5 (2 h) catalyst was tested for SB hydrolysis upon cycling. Fig. 7a shows the plot of the HGR normalized by the initial (HGR_0) as a function of the cycle number. Catalytic activity is retained during the first two cycles and then catalyst deactivates in cycle 3. As previously reported, a reactivation step consisting of washing the catalyst with diluted acid (10^{-4} M HCl) was employed after cycle 4. [20,31] This reactivation step aims to eliminate the B-O based species accumulated after each use, and has previously shown to be a deactivation mechanism for Co based catalysts for this reaction [20,31]. These B-O based species were detected in B1s and O1s levels together with Na 1s signal from XPS

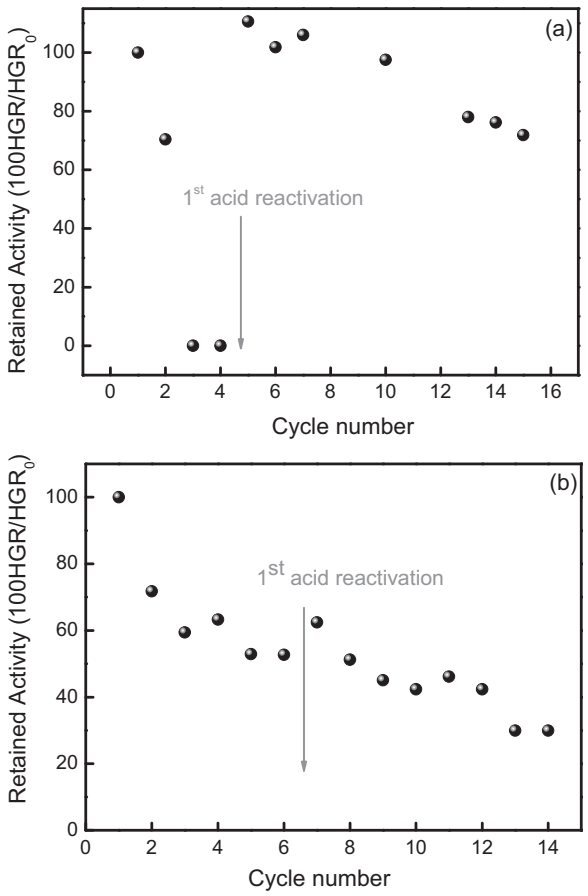

Fig. 7. Durability of the catalysts upon cycling. Retained activity as a function of the cycle number (HGR/HGR_0) (a) for SB hydrolysis (b) for AB hydrolysis.

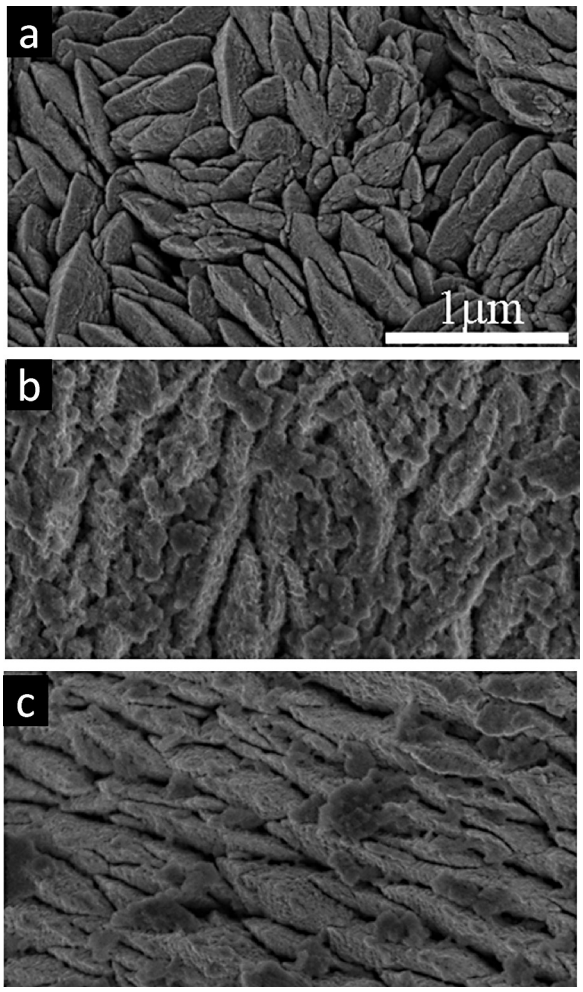

Fig. 8. Planar SEM images for the cycling experiments for 200 W Co 1.5 (2 h) catalyzed SB hydrolysis (a) Fresh catalyst (b) after 4 cycles (c) after 4 cycles washed with diluted acid.

on the used catalyst after cycle 4 (Table 3) and by SEM images as a film (Fig. 8b). After diluted acid washing, the catalytic activity was recovered (cycle 5) despite the XPS characteristic signals of B-O species were still present in the catalyst (191.9 eV, Table 3 bonds assigned according to Refs. [18,37]) and SEM micrographs (Fig. 8c) show partial recovery of the structural features of the fresh catalyst (Fig. 8a). Quantification of the XPS spectra permitted to calculate B/Co ratio before and after acid washing. Table 3 shows that this ratio is reduced three fold after acid washing (B/Co ratio 0.6 and 0.2 before and after acid washing). This indicates that the BO_2^- anion adsorbs strongly to the Co surface but small amounts of this anion do not interfere with activity. For the subsequent cycles, dilute acid washing was employed after each cycle. From cycle 5, catalytic activity decreases constantly within the experimental error to reach 76% of the initial after 14 cycles. This means that dilute acid (10^{-4} M HCl) washing may not be totally efficient to eliminate

Table 3
XPS analysis during cycling experiments on 200 W Co 1.5 (2 h) catalyst for sodium borohydride reaction.* Ratios obtained by the quantification of the corresponding levels in the XPS spectra.

Signal	Fresh catalyst	After cycle 4	After cycle 4 diluted acid washing
Co ($2p_{3/2}$)	777.8/780.9 eV (Co^0/Co-O)	780.9 eV	780.9 eV
O (1s)	529.33/531.7 eV (O-Co)	531.3 eV	531 eV
B (1s)	–	191.9 eV (BO_2^-)	191.5 eV
Na (1s)	–	1071.6 eV (Na-B-O)	–
*B/Co	–	0.608	0.2

B-O based species and they finally accumulate and stabilize after each cycle as previously shown [31]. More concentrated acid solutions could not be employed because leaching of the thin film is produced. The acid washing was previously tested at 1, 0.1, 0.001, 10^{-3} and 10^{-4} M. The latter concentration showed to be the less aggressive for the film. By weighting the supported catalysts before and after each test, no mass loss was found during 14 cycles within the experimental error. However, small losses should be evaluated by analyzing the acid solutions after each washing. These losses could be in part a reason for the deactivation, despite the use of reactivation steps.

3.4.2. Ammonia borane hydrolysis

Durability of the 50 W Co 2.8 (4 h) catalysts was evaluated for ammonia borane hydrolysis upon cycling. Results are shown in Fig. 7b. Catalyst deactivates after each run to reach 60% of its initial activity after 6 cycles. Taking into account reaction (2) one deactivation mechanism could also be the adsorption of B-O species as BO_2^- is the main hydrolysis product together with ammonium (and or ammonia depending the reaction pH). For this reason, as well as in Section 3.4.1, from cycle 6, after each cycle the catalyst was also washed with dilute acid in order to dissolve adsorbed borates (basic in nature) on Co surface and also ammonia in the form of ammonium cation ($pKa \sim 9$). Fig. 7b shows that in subsequent cycles the catalyst continued to deactivate, indicating no effect of the dilute acid washing. Fig. 9 shows SEM micrographs of

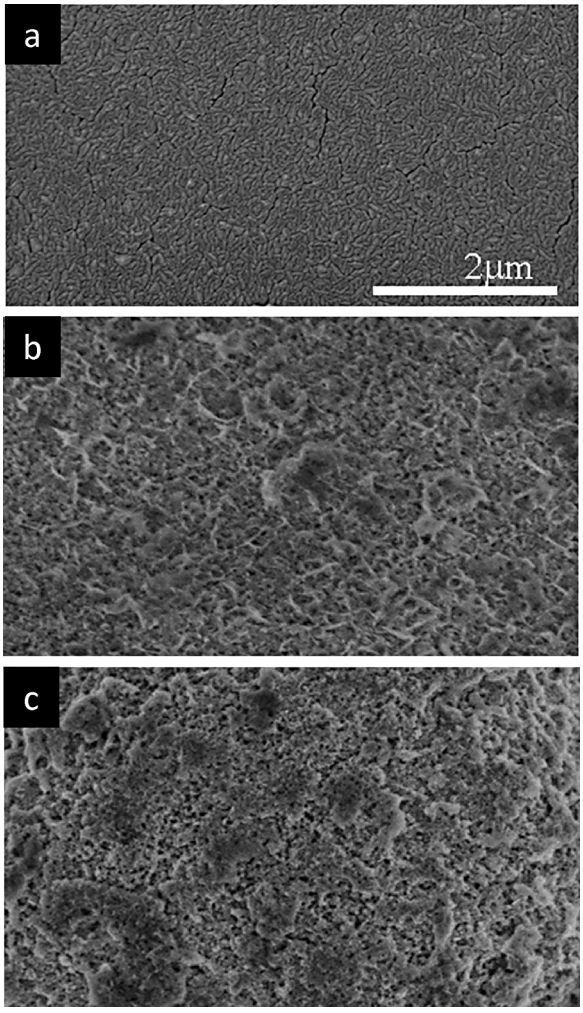

Fig. 9. Planar SEM images for the cycling experiments for 50 W Co 2.8 (4 h) catalyzed AB hydrolysis (a) Fresh catalyst (b) after 14 cycles (c) after 14 cycles washed with diluted acid.

50 W Co 2.8 (2 h) sample after cycle 14 before and after dilute acid washing in comparison with the fresh catalyst. Fig. 9b shows a film on catalyst surface that might block the access of ammonia borane to the catalyst during reaction. Acid washing was clearly not efficient in eliminating this film as shown in Fig. 9c. To understand this, the samples where studied by XPS. Table 4 summarizes main results (bonds assigned according to Refs. [18,37]). The persistence of Co-NH_3 signals in the N (1s) level (~399.6 eV) and Co-BO_2^- signals in the B (1s) level (~192 eV) for the acid washed catalyst indicates strong Co-adsorbate interactions that cannot be completely eliminated. However, Co-NH_3 interaction has shown to be stronger as demonstrated by the comparison of the N/Co ratio obtained by XPS before (0.3) and after (0.2) acidic washing in cycle 6 (Table 4). On the contrary Co-BO_2^- interactions were significantly eliminated by the acid washing as shown by quantitative XPS measurements (B/Co ratio 4 before cycle 6 and 0.68 after acid washing). These strong Co-NH_3 interactions have demonstrated to be stable upon acid washing. By weighting supported catalysts before and after each test, no mass loss was found during 14 cycles within the experimental error.

Table 4
XPS analysis during cycling experiments on 50 W Co 2.8 (4 h) catalyst for ammonia borane reaction.* Ratios obtained by the quantification of the corresponding levels in the XPS spectra.

Signal	Fresh Catalyst	After cycle 6	After cycle 6 Diluted acid washing
Co ($2p_{3/2}$)	777.8/780.8 eV (Co^0/Co-O)	781.8 eV	780.7 eV
O (1s)	529.33/531.7 eV (O-Co)	531.8 eV	531 eV
B (1s)	–	192.1 eV (BO_2^-)	191.8 eV
N (1s)	–	399.9eV(H_3N-Co)	399.6 eV
*B/Co	–	4	0.68
*N/Co	–	0.3	0.2

4. Conclusions

In this paper, supported Co catalysts were prepared for the first time as thin films by magnetron sputtering for SB and AB hydrolysis. The preparation technique has shown to be effective in depositing Co catalysts on metallic and polymeric supports which is highly advantageous for technological applications. Co thin films have demonstrated to be stable and well adhered to Ni foam in the reaction medium. Catalytic activity was improved by varying deposition conditions. Lowering deposition power and increasing deposition pressure was the strategy employed because it produces smaller crystallite size (more amorphous) and smaller column size (more disperse) materials. The highest catalytic activity was obtained for the 50 W Co 4.5 (4 h) sample and resulted in 2650 ml min^{-1} $g_{catalyst}{}^{-1}$ ($E_a = 60 \pm 2$ kJ mol^{-1}) for SB hydrolysis.

Durability of the prepared thin films was also tested for both reactions upon cycling. For SB hydrolysis, the tested catalyst has shown better durability than the one tested for AB hydrolysis. Basically, for SB hydrolysis, the adsorption of B-O based species is the main deactivation mechanism which has shown to be in part reversible by acid washing. For AB hydrolysis, NH_3 adsorption on Co surface demonstrated to be stronger than BO_2^- and resistant to acid washing.

Acknowledgements

Financial support from MINECO (CTQ2012-32519), CSIC (PIE 201260E006 and 201060E102), Junta de Andalucía (TEP217, PE2012-TEP862), the EC (CT-REGPOT-2011-1-285895, AL-NANOFUNC) is acknowledged. Authors would like to thank to Dr. Carmen López–Santos for the AFM measurements, and to the reviewers for their valuable comments.

Appendix A. Supplementary data

Supplementary data associated with this article can be found, in the online version, at http://dx.doi.org/10.1016/j.apcatb.2014.04.047.

References

[1] U.B. Demirci, O. Akdim, J. Andrieux, J. Hannauer, R. Chamoun, P. Miele, Fuel Cells 3 (2010) 335–350, References therein.
[2] S.S. Muir, X. Yao, Int. J. Hydrogen Energy 36 (2011) 5983–5997, References therein.
[3] B.H. Liu, Z.P. Li, J. Power Sources 187 (2) (2009) 527–534, References therein.
[4] H.L. Jiang, Q. Xu, Catal. Today 170 (2011) 56–63, References therein.
[5] U.B. Demirci, P. Miele, Phys. Chem. Chem. Phys. 12 (2010) 14651–14665, References therein.
[6] U.B. Demirci, O. Akdim, J. Andrieux, J. Hannauer, R. Chamoun, P. Miele, Sci. China Chem. (53) (2010) 1870–1879, References therein.
[7] U.B. Demirci, P. MIELE, Phys. Chem. Chem. Phys. (2014), http://dx.doi.org/10.1039/C4CP00250D.
[8] Ç. Çakanyildirim, M. Gürü, Renewable Energy 35 (2010) 839–844.
[9] W.H. Shin, S.H. Yang, Y.J. Choi, H.M. Jung, C.O. Song, J.K. Kang, J. Mater. Chem. 19 (2009) 4505–4509.
[10] W. Ye, H. Zhang, D. Xu, L. Ma, B. Yi, J. Power Sources 164 (2007) 544–548.
[11] N.A. Malvadkar, K. Sekeroglu, W.J. Dressik, M.C. Demirel, J. Power Sources 196 (2011) 8553–8560.

[12] H. Li, J. Liao, X. Zhang, W. Liao, L. Wen, J. Yang, H. Wang, R. Wang, J. Power Sources 239 (2013) 277–283.
[13] T. Umegaki, J.M. Yan, X.B. Zhang, H. Shioyama, N. Kuriyama, Q. Xu, J. Power Sources 195 (2010) 8209–8214.
[14] Q. Xu, M. Chandra, J. Power Sources 163 (2006) 364–370.
[15] F. Wu, Y. Wu, B. Bai, Yi H. Zhang, Mater. Lett. 59 (2005) 1748–1751.
[16] H. Tian, Q. Guo, D. Xu, J. Power Sources 195 (2010) 2136–2142.
[17] R. Fernandes, N. Patel, A. Miotello, R. Jaiswal, D.C. Kothari, Int. J. Hydrogen Energy 36 (2011) 13379.
[18] G.M. Arzac, T.C. Rojas, A. Fernández, ChemCatChem 3 (2011) 1305–1313.
[19] O. Akdim, R. Chamoun, U.B. Demirci, Y. Zaatar, A. Khoury, P. Miele, Int. J. Hydrogen Energy 36 (2011) 14527–14533.
[20] O. Akdim, U.B. Demirci, P. Miele, Int. J. Hydrogen Energy 36 (2011) 13669–13675.
[21] N. Patel, R. Fernandes, G. Guella, A. Kale, A. Miotello, B. Patton, C. Zanchetta, J. Phys. Chem. C 112 (2008) 6968–6976.
[22] N. Patel, G. Guella, A. Kale, A. Miotello, B. Patton, C. Zanchetta, L. Mirengui, P. Rotolo, Appl. Catal., A: Gen. 323 (2007) 18–24.
[23] N. Patel, A. Miotello, V. Bello, Appl. Catal., B: Environ. 103 (2011) 31–38.
[24] N. Patel, R. Fernandes, A. Santini, A. Miotello, Int. J. Hydrogen Energy 37 (2012) 2007–2013.
[25] H.S. Nagaraja, J. Supercond. Novel Magn. 25 (2012) 1901–1906.
[26] V. Godinho, T.C. Rojas, A. Fernández, Microporous Mesoporous Mater. 149 (2012) 142–146.
[27] V. Godinho, C. Lopéz-Santos, T.C. Rojas, D. Philippon, M.C. Jimenez de Haro, S. Lucas, A. Fernandez, J. Alloys Compd. 536 (2012) S398–S406.
[28] V. Godinho, J. Caballero-Hernández, D. Jamon, T.C. Rojas, R. Schierholz, J. García-López, F.J. Ferrer, A. Fernández, Nanotechnology 24 (2013), 275604 (10pp).
[29] E. Young, D.G. Nocera, V. Bulovic, Energy Environ. Sci. 3 (2010) 1726–1728.
[30] I. Horcas, R. Fernández, J.M. Gómez-Rodríguez, J. Colchero, J. Gómez-Herrero, A.M. Baro, Rev. Sci. Instrum. 78 (2007) 013705.
[31] G.M. Arzac, D. Hufschmidt, M.C. Jiménez de Haro, A. Fernández, B. Sarmiento, M.A. Jiménez, M.M. Jiménez, Int. J. Hydrogen Energy 37 (2012) 14373–14381.
[32] J.A. Thornton, Annu. Rev. Mater. Sci. 7 (1977) 239–260.
[33] G.W. Qin, B. Yang, N. Xiao, Y.P. Ren, M. Jiang, X. Zhao, K. Oikawa, Thin Solid Films 517 (2009) 2984–2987.
[34] B. Sen, C.M. Kaufman, Chem. Soc. Dalton Trans. 64 (1985) 307–313.
[35] J.C. Walter, A. Zurawski, D. Montgomery, M. Thornburg, S. Revankar, J. Power Sources 179 (2008) 335–339.
[36] K.A. Holbrook, P.J. Twist, J. Chem. Soc. A (1971) 890–894.
[37] A. Galtyries, E. Laksono, J.-M. Siffre, C. Argile, P. Marcus, Surf. Interface Anal. 30 (2000) 140–144.